RSC Advances

PAPER

View Article Online
View Journal | View Issue

Cite this: *RSC Adv.*, 2017, **7**, 48994

Effect of the BN content on the thermal shock resistance and properties of BN/SiO_2 composites fabricated from mechanically alloyed SiBON powders

Quan Li,[a] Zhihua Yang,*[ab] Yang Miao,[a] Bin Liang,[a] Delong Cai,[a] Shengjin Wang,[a] Xiaoming Duan,[ab] Dechang Jia*[ab] and Yu Zhou[a]

Wave-transparent composites of BN/SiO_2 were prepared *via* hot pressure sintering at 1650 °C of mechanically alloyed amorphous SiBON powders. The mechanical, dielectric and thermal properties and thermal shock resistance of the composites were carefully investigated with different BN contents. With increasing BN content, the flexural strength and fracture toughness of the composites increased first and then decreased. The sample with the composition of SiO_2–5BN exhibited the highest flexural strength of 256.3 MPa and a fracture toughness of 3.15 MPa $m^{1/2}$. The relative density decreased with the increase of BN content, which would influence the thermal properties and the thermal shock resistance of the composites. The formation of borosilicate glass and crystallization of fused silica in the surface at the high temperature greatly improved thermal shock resistance of the samples. The SiO_2–6BN sample, possessing low relative density, exhibited the best thermal shock resistance, and the retained strength after a thermal shock of 1100 °C was 98.6% of the original strength. Besides excellent mechanical and thermal properties and thermal shock resistance, the as-sintered composites exhibited low dielectric constant (ε < 4.62) and loss tangent (tan δ < 0.002), meeting the required values for high temperature wave-transparent materials.

Received 6th September 2017
Accepted 25th September 2017

DOI: 10.1039/c7ra09905c

rsc.li/rsc-advances

1 Introduction

Continuous rapid developments in the aerospace industry provide an impetus to the increasing demand for advanced materials with enhanced properties. Structural parts and components must meet more severe design constraints, such as good mechanical and dielectric properties, excellent thermal shock resistance and very high ablation resistance, when operated in extreme environments.[1–3] Among the various structural materials, h-BN ceramics with high melting points (>3000 °C), high refractoriness, good ablation resistance, low dielectric coefficient and loss tangent (5.16 and 10–11 × 10^{-4}, respectively, at room temperature), excellent thermal shock resistance, and good machinability[4–6] are suggested to be a suitable candidate for antenna and radome window materials on carrier-rockets, airships and missiles.[7,8] However, the poor sinterability and mechanical properties as well as weak oxidation resistance have limited the application of single-phase h-BN materials. Hence, improvements in the sinterability and mechanical properties of hexagonal boron nitride have been the main issues in the past decades.[9–11]

Adding compounds such as SiO_2, Al_2O_3, MAS (magnesium aluminum silicate) and YAG (yttrium aluminum garnet) is an effective way to improve the sinterability of BN ceramics.[12–14] Among these, fused silica is the excellent one, notably improving the sintering characteristics, with rather low and stable dielectric constant (ε < 3.5), and very low loss tangent, low coefficient of thermal expansion, and high melting point (1700 °C).[15–19] Furthermore, appropriate pretreatment could be used to overcome the drawbacks. Our previous work showed that sinterability of h-BN powders can be notably improved *via* boll milling.[20] And mechanical alloying is a synthesis method to form amorphous powders with low cost and simple procedures.[21,22] Thus, it may be a useful method to further improve the sinterability of BN composites to achieve high relative densities and good mechanical properties.

Up to now, the studies of the dielectric and thermal properties and thermal shock resistance of the BN/SiO_2 composites have been scarce. Further studies are still essential to find out the mechanism of the co-operative enhancement of the relevant properties in the composites. In this work, a series of mechanically alloyed amorphous SiBON powders with

[a]*Institute for Advanced Ceramics, School of Materials Science and Engineering, Harbin Institute of Technology, Harbin, Heilongjiang, 150080, P. R. China. E-mail: zhyang@hit.edu.cn; dcjia@hit.edu.cn; Fax: +86 0451 86414291; Tel: +86 0451 86418792*

[b]*State Key Laboratory of Advanced Welding and Joining, School of Materials Science and Engineering, Harbin Institute of Technology, P. O. Box 433, Harbin, Heilongjiang, 150001, P. R. China*

different BN content were prepared, and then hot pressed to dense bulk ceramics. The effects of BN content on mechanical, dielectric and thermal properties of the composites were studied. The effects of the crystallization of amorphous SiO_2 and the oxidation of h-BN on thermal shock resistance are also discussed.

2 Materials and methods

Hexagonal BN (1.31 μm, 99.5% purity, Advanced Technology & Materials Co. Ltd, Beijing, P. R. China) and fused silica (0.9 μm, 98.0% purity, Guangyu Quartz Co. Ltd, Lianyungang, P. R. China) were used as starting materials. A series of amorphous SiBON powders, with chemical composition varying from 1 : 0.5 to ~1 : 7 SiO_2 : h-BN (molar ratio), were synthesized using a vario-planetary mill (FRITSCH P4, FRITSCH (Beijing, P. R. China) Scientific Instruments Co., Ltd, Germany). Then the amorphous powders were put into graphite dies and hot-press sintered under a pressure of 20 MPa for 0.5 h at 1650 °C in 1 atm N_2 atmosphere. Samples were given brief names, for instance, SiO_2 : BN = 1 : 0.5 was labeled S0.5BN.

Density was calculated according to the Archimedes principle, and the relative density calculated by division of density by theoretical density. The fabricated samples were ground and polished with 0.4 μm SiC abrasive paper and diamond suspension. Flexural strength was tested by the three-point bending method using rectangular bars (3 mm × 4 mm × 36 mm) in a universal testing machine (Istron-5569, Instron Group, USA) with a span of 30 mm and a cross-head speed of 0.5 mm min^{-1}. Fracture toughness measurement was performed on single-edge-notched beams (2 mm × 4 mm × 20 mm) with a span of 16 mm at a cross-head speed of 0.05 mm min^{-1}, and a half-thickness notch was made using a 0.1 mm thick diamond wafer blade. Vicker's hardness was measured with a load of 5 kg using an HBV-30A tester. The thermal shock resistance was evaluated by water quenching experiments. Five samples were used for each mechanical property measurement and the average values are reported.

Phase analysis was evaluated by X-ray diffraction (XRD; RigakuD/Max 2200VPC, Japan) at a scan rate of 4° per min. The microstructures were examined by scanning electron microscopy (SEM; Quanta 200, FEI Co., USA). Dielectric constant and loss tangent of the samples (Φ 50.0 mm × 2.0 mm) were measured in the frequency range of 7 GHz to 18 GHz at room temperature by RF impedance/material analyzer (PNA N5230A, Agilent, USA). The thermal conductivity (TC) of the samples with a size of Φ 12.6 mm × 1 mm was measured at ~25–1200 °C by LFA laser apparatus (NETZSCH LFA427, Germany). The coefficient of thermal expansion (CTE) was measured with samples of 4 mm × 4 mm × 10 mm at ~200–1400 °C (NETZSCH DIL402C, Germany).

3 Results and discussion

3.1. Microstructure and mechanical properties

Fig. 1(a) shows the XRD patterns of as-sintered SiBON composites, indicating that h-BN crystallized from the amorphous SiBON powders. The intensity of the h-BN planes increased with increasing BN content. Fig. 1(b) shows the XRD patterns of S0.5BN and S5BN samples taken in two directions. The side and top surface, measured perpendicular and parallel to the hot-press sintering direction, are denoted as ⊥ and ||, respectively. The diffraction intensity of the (002) plane was great higher than that of the (100) plane on the top surface, while the diffraction intensity of the (002) plane was about the same value as for the (100) plane on the side surface. This indicated the h-BN exhibited a degree of orientation in the composites.

In order to discuss the effects of BN content on the bulk orientation of the samples, the following formula was applied:[23]

$$\mathrm{IOP} = \begin{cases} \dfrac{(I_{100}/I_{002})\mathrm{perp}}{(I'_{100}/I'_{002})\mathrm{par}}, & \text{when}(I_{100}/I_{002})\mathrm{perp} > (I'_{100}/I'_{002})\mathrm{par} \\ -\dfrac{(I'_{100}/I'_{002})\mathrm{par}}{(I_{100}/I_{002})\mathrm{perp}}, & \text{when}(I_{100}/I_{002})\mathrm{perp} < (I'_{100}/I'_{002})\mathrm{par} \end{cases} \quad (1)$$

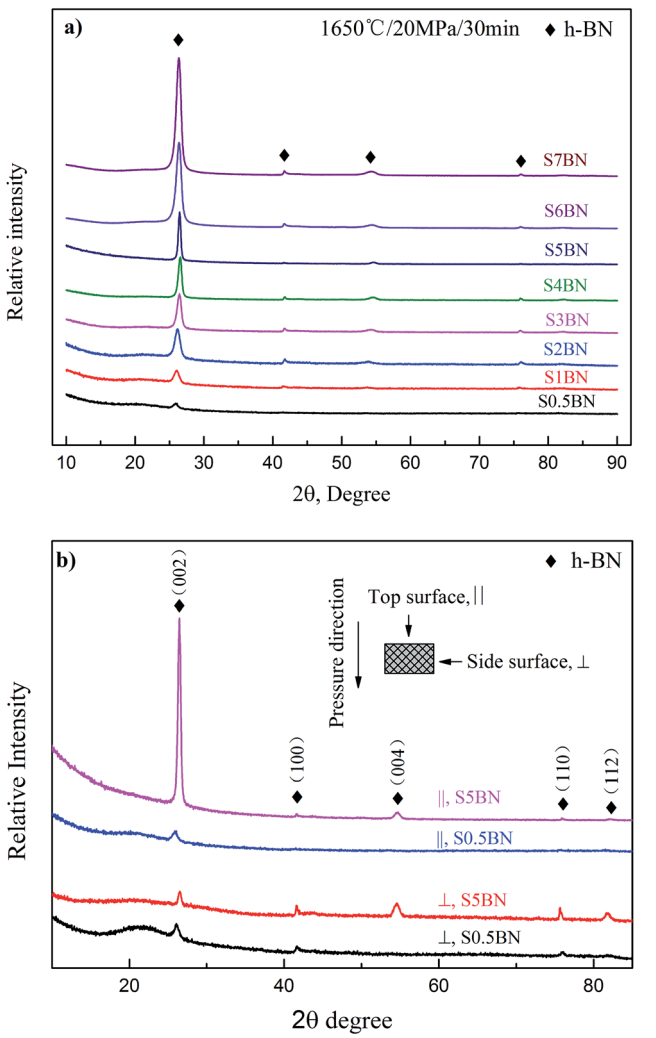

Fig. 1 (a) XRD patterns of SiBON ceramics sintered at 1650 °C under 20 MPa for 0.5 h; (b) XRD patterns of S0.5BN and S5BN were taken along two directions.

Table 1 IOP index of BN/SiO_2 composite ceramics with different BN content

Samples	S0.5BN	S1BN	S2BN	S3BN	S4BN	S5BN	S6BN	S7BN
IOP index	1.72	1.96	2.89	6.22	8.61	25.6	25.8	26.7

where IOP is the index of orientation preference, and I_{hkl} and I'_{hkl} are the intensities of corresponding diffraction lines measured in the ceramics for the surfaces perpendicular and parallel to the pressure axis, respectively. Furthermore, when IOP equals ±1, the BN grains are orientated randomly. An IOP value > 1 means that the *c*-axis of the h-BN lattice is preferentially orientated perpendicular to the hot-pressing direction. The larger the IOP value, the more h-BN grains have their *c*-axis orientated perpendicular to the hot-pressing direction. The IOP values of the samples are shown in Table 1, which indicates that the IOP value increases from 1.72 to 26.7 with the increasing BN content. Under the condition of enough liquid phase in the process of densification, increasing BN content can increase the contact chances of BN particles, which will promote the growth of BN flakes with preferred orientation.

The relative density and mechanical properties of the composite ceramics are listed in Table 2. The relative density declined from 97.2% to 91.1% with increasing BN content from 0.5 to 7 in the SiO_2 : BN ratio. The flexural strength and fracture toughness increased first and then decreased, with the sample of S5BN exhibiting the highest flexural strength of 256.3 MPa and fracture toughness of 3.15 MPa $m^{1/2}$, respectively. Attributed to the high relative density, the preferential orientation of the flaked BN grains and the desirable interfacial stresses between BN and SiO_2, the strength and toughness of the composite ceramics were obviously increased compared with pure fused silica or h-BN. Moreover, mechanically alloyed amorphous SiBON powders gave homogeneous distribution and sufficient contact of the different components in the composites, which was favorable to mechanical properties.

Fig. 2 shows the morphology of the fracture surface of samples with different BN content, consisting of crystallized BN and amorphous phase. It can be seen that the sizes of BN grains generally increased with the increase of BN content. Fig. 3(a) and (b) shows the morphology of the fracture surface of S3BN and the sample of the same composition without pretreatment by mechanical alloying, indicating particle sizes of BN in S3BN notably smaller than in the boll-milled sample, which is ascribed to the homogeneous distribution of the different components. As the flaked grains were crystallized BN, energy dispersive X-ray spectroscopy (EDS) measurement was carried out to confirm the composition of the amorphous phase, shown in Fig. 3(c) and (d). Because of the good chemical compatibility between the SiO_2 and BN reported previously,[19] combined with the results of EDS analysis, we assumed that the amorphous phase consisted of mainly SiO_2, non-crystallized BN and a little B_2O_3 formed during the mechanical alloying procedure. Since its coefficient of thermal expansion is slightly lower than that of BN, fused silica always suffers from compressive stress at the interface in composites; therefore, it could be strengthened by the addition of BN. When the BN/SiO_2 ratio was larger than 3, the pull-out of a large number of small BN platelets could be observed.

The elastic modulus of sintered composites shows the same trend as relative density. Generally, lower hardness leads to easier machinability. The hardness of the samples decreased with increasing BN content; when the BN/SiO_2 ratio of the composite was 4, the Vickers hardness was 2.97 GPa, which is lower than that of machinable mica-glass-ceramic (3 GPa).[24]

3.2. Thermal properties

Generally, thermal conductivity (TC) of the composites could be affected by the composition, microstructure and porosity of the composites. The TC (phonon TC, λ_P) of BN/SiO_2 composites could be approximately expressed by the following formula:[25]

$$\lambda_p = \frac{1}{3} C v_p l_p \quad (2)$$

where C is the heat capacity, v_p is the phonon velocity and l_p is the phonon MFP (mean free path). As the porosity increased monotonically with increasing BN content of the composites, four samples (S1BN, S3BN, S5BN, S7BN) were selected to test the TC values, with the temperature varying from 25 to 1200 °C. As shown in Fig. 4(a), with the increase of temperature, the frequency of phonon scattering increased and the phonon MFP decreased, which resulted in a decrease of TC. Although the relative density of samples decreased with the increasing of BN content, which would be expected to lead to a lower TC value,

Table 2 Some properties of the HP sintered BN/SiO_2 ceramics

Samples	Density (g cm^{-3})	Relative density (%)	Flexural strength (MPa)	Elastic modulus (GPa)	Vickers hardness (GPa)	Fracture toughness (Mpa $m^{1/2}$)
S0.5BN	2.14	97.2	163.0 ± 8.4	72.8 ± 4.6	5.05 ± 0.05	1.59 ± 0.17
S1BN	2.15	97.1	186.4 ± 9.5	68.3 ± 6.8	4.23 ± 0.08	2.08 ± 0.08
S2BN	2.15	96.8	191.6 ± 10.3	63.9 ± 4.8	3.47 ± 0.01	2.51 ± 0.12
S3BN	2.15	96.7	198.7 ± 9.9	51.6 ± 3.6	3.10 ± 0.04	2.66 ± 0.03
S4BN	2.16	96.8	225.3 ± 13.4	52.7 ± 5.2	2.97 ± 0.05	2.90 ± 0.12
S5BN	2.12	95.0	256.3 ± 6.5	51.4 ± 2.1	2.39 ± 0.01	3.15 ± 0.15
S6BN	2.08	93.1	212.2 ± 13.5	50.6 ± 3.2	1.89 ± 0.01	2.45 ± 0.24
S7BN	2.04	91.1	205.1 ± 11.3	47.3 ± 4.3	1.67 ± 0.23	2.10 ± 0.31

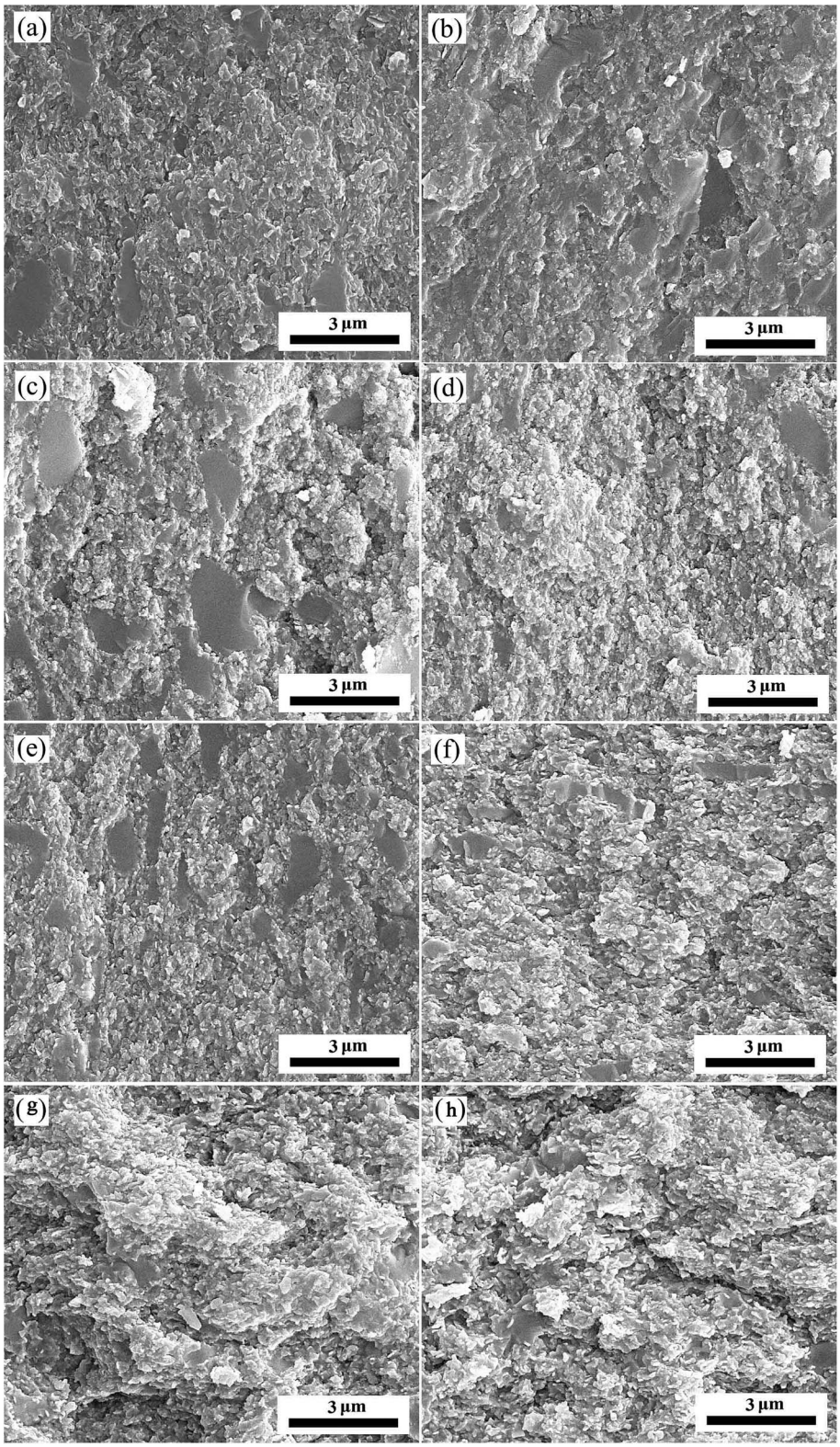

Fig. 2 Fracture morphology images of (a) S0.5BN; (b) S1BN; (c) S2BN; (d) S3BN; (e) S4BN; (f) S5BN; (g) S6BN; (h) S7BN.

while the TC value of BN is larger than that of fused silica (0.5 W $m^{-1} \cdot K^{-1}$), the TC value of samples generally increased with the increasing BN content, and the samples' TC values are about 0.85–3.66 W $m^{-1} \cdot K^{-1}$ at ~200–1200 °C in general.

Fig. 4(b) shows the coefficient of thermal expansion (CTE) values of S1BN, S3BN, S5BN and S7BN with the temperature varying from 200 to 1400 °C. The CTE values increased with increasing of temperature. The CTE values of h-BN

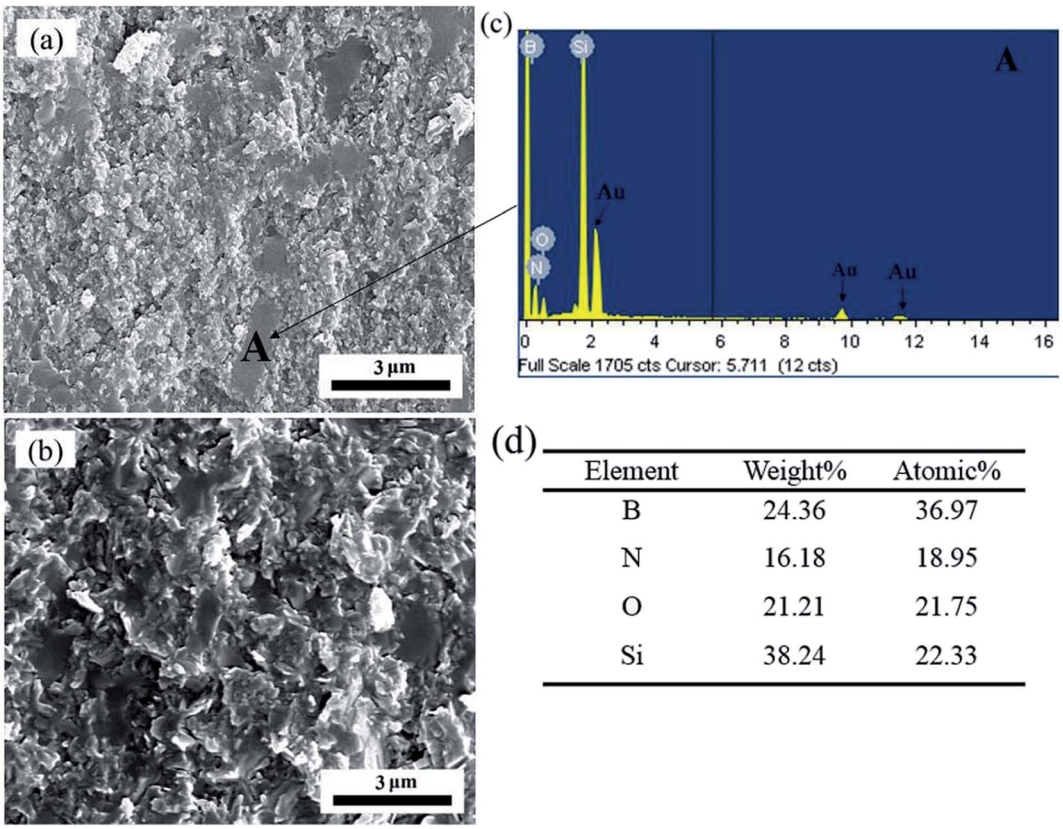

Element	Weight%	Atomic%
B	24.36	36.97
N	16.18	18.95
O	21.21	21.75
Si	38.24	22.33

Fig. 3 (a) Fracture morphology image of S3BN; (b) fracture morphology image of 3BN–SiO_2 fabricated from the powders without mechanical alloying pretreatment; (c) EDS analysis of the A zone in (a); (d) chemical composition of the A zone in (a) from the EDS analysis.

(0.7×10^{-6} K^{-1} ($\perp$) and 2.7×10^{-6} K^{-1} ($\parallel$)) are a little larger than fused silica (0.54×10^{-6} K^{-1}), and the CTE value of the samples increased with the increase of BN content. As fused silica and h-BN constitute the main phase in the samples, the composites have low CTE values of ~0.35–4.71 $\times 10^{-6}$ K^{-1} in the temperature range ~200–1400 °C, which makes BN/SiO_2 composite ceramics a promising candidate with excellent thermal shock resistance.

3.3. Thermal shock resistance

The important measure of the thermal shock resistance is the residual strength of material after water quenching, according to Kingery's theory of critical stress.[26] The retained strength of the samples after water quenching at 800–1100 °C is shown in Fig. 5, which indicates that the BN/SiO_2 composite ceramics showed excellent thermal shock resistance compared with other BN-based composites.[27] When the ratio of the BN/SiO_2 varied from 2 to 6, the residual flexural strength of samples decreased when the temperature difference (ΔT) was below 1000 °C, but a maximum appeared at 1000 °C, and then values decreased with further increase in the temperature difference. When the ratios of the BN/SiO_2 were 1 and 7, the curves of residual flexural strength were different from the others.

Since porous ceramics had better thermal shock resistance than the dense material,[28] S6BN with low relative density exhibited excellent thermal shock resistance. The retained strength values after thermal shock of 1000 °C and 1100 °C were 227.5 and 209.3 MPa, which were 107.1% and 98.6% of the original strength, respectively. In an inert atmosphere, h-BN will be stable and could retain its mechanical properties up to temperatures in excess of 2000 °C.[29] However, BN reacts with oxygen to form B_2O_3 at low temperatures (<450 °C) in an oxidizing environment. Further increase of the temperature (>1100 °C) would cause noticeable vaporization of B_2O_3 and cause bubbles to form on the surface of the composites. The reactions can be described as follows:[30]

$$4BN(s) + 3O_2(g) = 2B_2O_3(l) + 2N_2(g) \quad (3)$$

$$B_2O_3(l) = B_2O_3(g) \quad (4)$$

At high temperatures, the oxidation-derived B_2O_3 could come into contact with SiO_2 and produce a viscous borosilicate glass coating BN particles to prevent the oxidation of BN.[31] Fig. 6 shows the surface of S6BN after water quenching at 800–1100 °C, indicating the surfaces of samples were dense and smooth, which explained why the retained strengths of the composites were a little higher than the original strengths after quenching at temperatures of 800–1100 °C. When the quenching temperature is higher than 900 °C, there are rod-like crystals formed at the surface of the sample, as shown in Fig. 6(b)–(d), which could

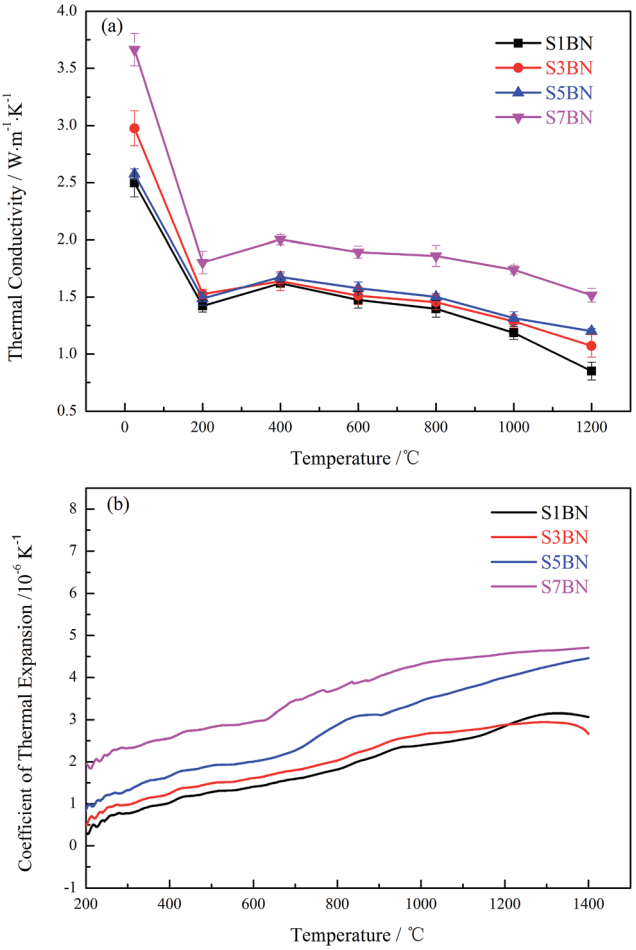

Fig. 4 Thermal properties of the samples variation with temperature: TC (a) and CTE (b).

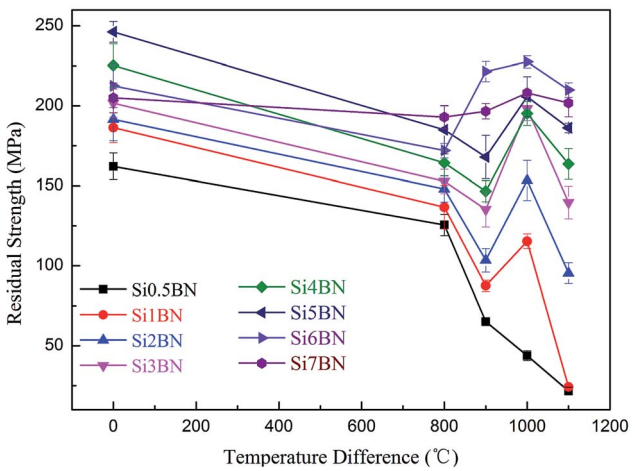

Fig. 5 Retained strength of the samples after water quenching at 800–1100 °C.

strongly increase the retained strengths; the rod-like crystals were observed in only the samples of S6BN and S7BN when all samples were water quenched at 900 °C. This may be responsible for the high retained strength of S6BN and S7BN water quenched at 900 °C, while that of the others decreased notably. For ΔT up to 1100 °C, vaporization of B_2O_3 occurred and bubbles formed on the surface were easily seen, as shown in Fig. 6(d), causing a decrease of the retained strengths. XRD and EDS measurements were applied to confirm the presence of the crystal phase and determine the composition of the rod-like crystals formed on the surface of S6BN after quenching at 1000 °C, as shown in Fig. 7. The XRD pattern illustrated that SiO_2 (JCPDF #31-1234, SiO_2-phase X2) had crystallized from the amorphous phase in S6BN. Furthermore, the composition of the rod-like SiO_2 was also proved by the results of the EDS analysis, indicating that the crystals consisted of Si and O elements in the atomic ratio of 3.5 : 6.5, which is near to 1 : 2. In order to check whether the rod-like SiO_2 formed in the body of the samples, fracture morphology images of samples with quenching temperatures of 800–1100 °C were observed (Fig. 8). Compared with the surface, there was not enough space for the growth of the rod-like SiO_2 in the dense body of the samples, which caused that the rod-like SiO_2 only to be distributed in the superficial layers.

Fig. 9 shows the SEM images of samples after water quenching at 1000 °C. It indicates that only the S0.5BN was without rod-like SiO_2 formed in the surface while other samples formed varying amounts, which may be the reason that the retained strength of S0.5BN always decreased with increasing ΔT, while a maximum of retained strength appeared at 1000 °C in other samples, as shown in Fig. 5. In short, the forming of the rod-like SiO_2 and the viscous borosilicate glass layer together maintained the retained strengths of the composites at high levels.

3.4. Dielectric property

Besides mechanical properties and thermal shock resistance, dielectric constant and loss tangent are significant performance parameters for wave-transparent applications. Generally, relative density (porosity) and phase composition are the two factors affecting the dielectric properties of BN/SiO_2 composites. The influences of these factors on dielectric constant can be represented by Lichtenecker's mixture law:[32]

$$\ln\varepsilon = \nu_{SiO_2}\cdot\ln\varepsilon_{SiO_2} + \nu_{h\text{-}BN}\cdot\ln\varepsilon_{h\text{-}BN} + \nu_{vac}\cdot\ln\varepsilon_{vac} \quad (5)$$

Here, ε represents the dielectric constant of the BN/SiO_2 composites, and $\varepsilon_{SiO_2(h\text{-}BN,\ vac)}$ and $\nu_{SiO_2(h\text{-}BN,\ vac)}$ denote the dielectric constant and volume fraction of the SiO_2, h-BN, and pores, respectively. The orders of their ε and tan δ are BN > SiO_2 > pores, and the ε and tan δ of pores can be regarded as 1 and 0 separately.[33] So the dielectric constant will increase with increasing BN content, and decrease with decreasing relative density of the composites.

Fig. 10(a) and (b) indicate the dielectric constant (ε) and loss tangent (tan δ) of the BN/SiO_2 composites, respectively. All the samples exhibit both low dielectric constant (ε < 4.62) and loss tangent (tan δ < 0.0020), acceptable for radome application. In general, the effects of BN content and the relative density on dielectric properties fit well with the mixture law. The sample S5BN with 95% relative density exhibited the maximum of dielectric constant of 4.62.

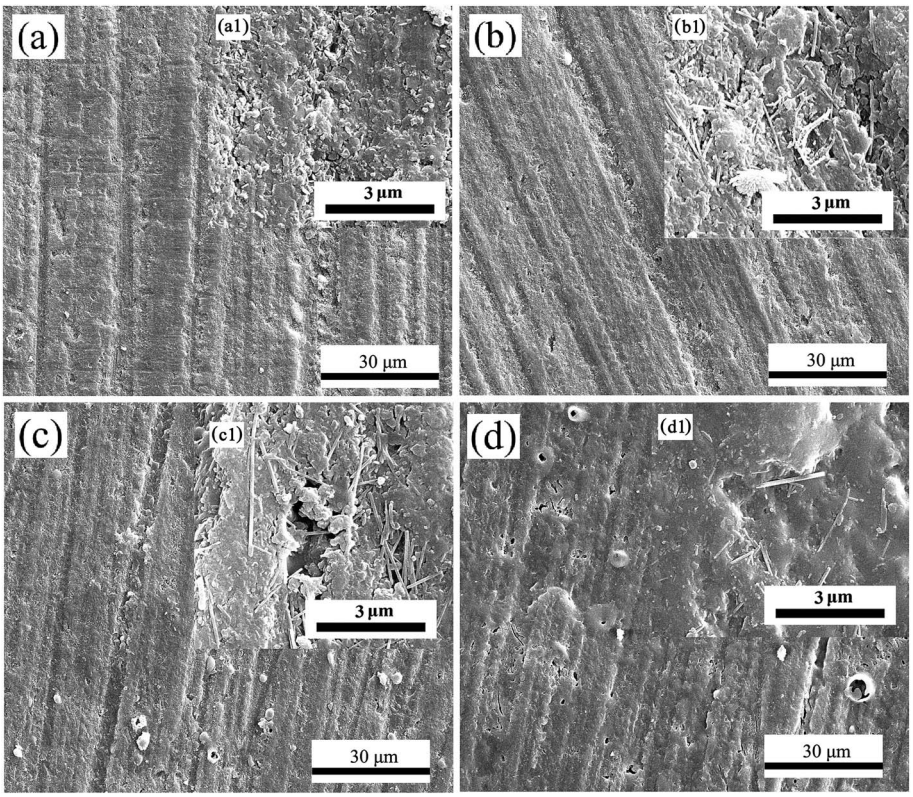

Fig. 6 SEM images of the surface of S6BN after water quenching at: (a) 800 °C; (b) 900 °C; (c) 1000 °C; (d) 1100 °C.

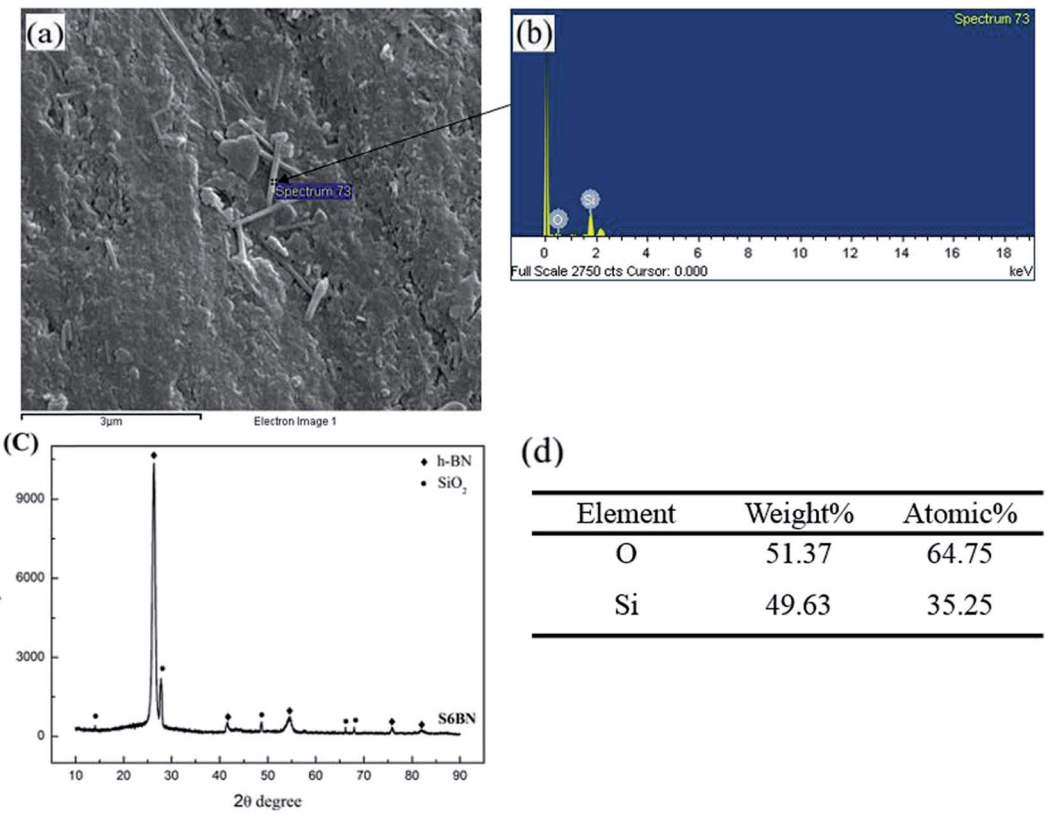

(d)

Element	Weight%	Atomic%
O	51.37	64.75
Si	49.63	35.25

Fig. 7 (a) SEM image of the surface of S6BN after water quenching at 900 °C; (b) EDS analysis of the marked rod-like grains; (c) the XRD pattern of S6BN after water quenching at 900 °C; (d) chemical composition of rod-like grains from the EDS analysis.

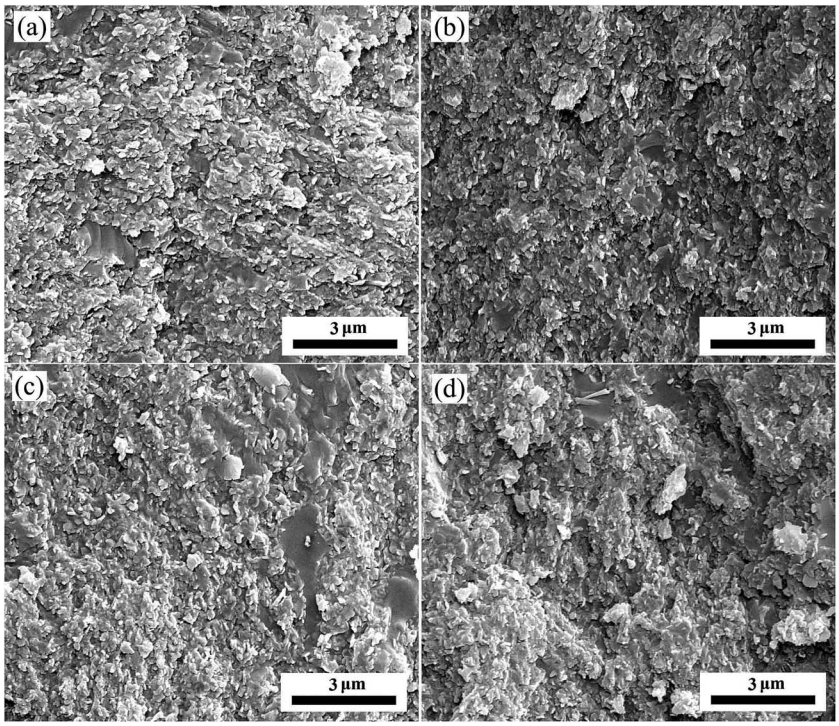

Fig. 8 Fracture morphology images of S6BN quenching temperature at: (a) 800 °C; (b) 900 °C; (c) 1000 °C; (d) 1100 °C.

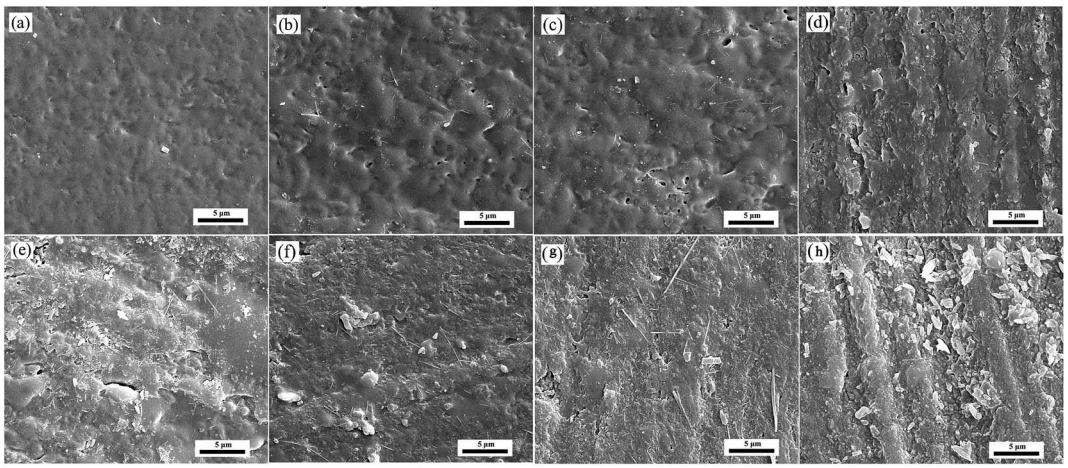

Fig. 9 SEM images of samples after water quenching at 1000 °C with different BN content: (a) S0.5BN; (b) S1BN; (c) S2BN; (d) S3BN; (e) S4BN; (f) S5BN; (g) S6BN; (h) S7BN.

4 Conclusions

In this study, BN/SiO_2 ceramic composites with different contents of BN were fabricated by hot pressure sintering of amorphous SiBON powders. The mechanical properties and dielectric properties both increased first and then decreased with the increasing content of BN, varying from 163.0 to 256.3 MPa (flexural strength) and 3.89 to 4.62 (ε), respectively. The composite ceramics have low CT and CTE values, the values increasing with increasing BN content. The thermal shock resistance of the composites could be enhanced by the borosilicate glass formed at high temperatures, which would seal the cracks and pores on the surface and protect the BN from oxidation damage, and the crystallization of SiO_2 at some temperature could greatly improve the thermal shock resistance. S6BN with the lowest relative density exhibited the best thermal shock resistance, and the retained strength after a thermal shock of 1100 °C is 98.6% of the original strength. So, it is believed that BN/SiO_2 composite ceramics are a promising candidate to use as high temperature wave-transparent materials.

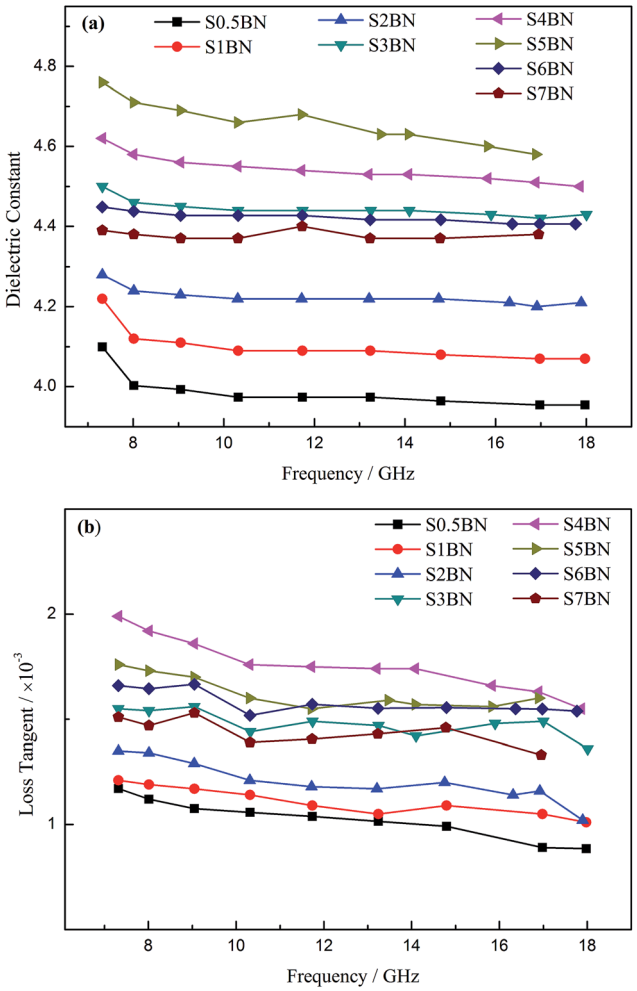

Fig. 10 Dielectric properties of the samples: (a) dielectric constant and (b) loss tangent.

Conflicts of interest

There are no conflicts to declare.

Acknowledgements

This work was supported by the National Natural Science Foundation of China (No. 51321061, 51372050, 51225203 and 51402068).

References

1 C. R. Zou, C. R. Zhang, B. Li, S. Q. Wang, Z. F. Xie and Y. C. Song, Ablation behavior of boron nitride based ceramic composites reinforced by continuous silicon oxynitride fiber, *Ceram. Int.*, 2015, **41**, 4768–4774.

2 N. N. Long, J. Q. Bi, W. L. Wang, M. Du and Y. J. Bai, Mechanical properties and microstructure of porous BN–SiO_2–Si_3N_4 composite ceramics, *Ceram. Int.*, 2012, **38**, 2381–2387.

3 X. M. Duan, D. C. Jia, Q. C. Meng, Z. H. Yang, Y. Yu, Y. Zhou, D. R. Yu and Y. J. Ding, Study on the plasma erosion resistance of ZrO_{2p}(3Y)/BN–SiO_2 composite ceramics, *Composites, Part B*, 2013, **46**, 130–134.

4 X. L. Li, X. P. Hao, M. W. Zhao, Y. Z. Wu, J. X. Yang, Y. P. Tian and G. D. Qian, Exfoliation of hexagonal boron nitride by molten hydroxides, *Adv. Mater.*, 2013, **25**, 2200–2204.

5 C. Steinborn, M. Herrmann, U. Keitel, A. Schonecker, J. Rathel, D. Rafaja and J. Eichler, Correlation between microstructure and electrical resistivity of hexagonal boron nitride ceramics, *J. Eur. Ceram. Soc.*, 2013, **33**, 1225–1235.

6 W. Sinclair and H. Simmons, Microstructure and thermal-shock behavior of BN composites, *J. Mater. Sci. Lett.*, 1987, **6**, 627–629.

7 J. L. Qi, J. H. Lin and Y. H. Wan, Joining of SiO_2–BN ceramic to Nb using a CNT reinforced brazing alloy, *RSC Adv.*, 2014, **4**, 64238–64243.

8 D. C. Jia, Y. Zhou and T. C. Lei, Ambient and elevated temperature mechanical properties of hot-pressed fused silica matrix composite, *J. Eur. Ceram. Soc.*, 2003, **23**, 801–808.

9 J. Eichler and C. Lesniak, Boron nitride (BN) and BN composites for high temperature applications, *J. Eur. Ceram. Soc.*, 2008, **28**, 1105–1109.

10 H. Lorenz and I. Orgzall, Influence of the initial crystallinity on the high pressure high temperature phase transition in boron nitride, *Acta Mater.*, 2004, **52**, 1909–1916.

11 Y. Meng, H. K. Mao, P. J. Eng, T. P. Trainor, M. Newville, M. Y. Hu, C. C. Kao, J. F. Shu, D. Hausermann and R. J. Hemley, The formation of sp(3) bonding in compressed BN, *Nat. Mater.*, 2004, **3**, 111–114.

12 C. Steinborn, M. Herrmann, U. Keitel, A. Schonecker, J. Rathel, D. Rafaja and J. Eichler, Correlation between microstructure and electrical resistivity of hexagonal boron nitride ceramics, *J. Eur. Ceram. Soc.*, 2013, **33**, 1225–1235.

13 D. Cai, Z. Yang, X. Duan, B. Liang, Q. Li, D. Jia and Y. Zhou, A novel BN-MAS system composite ceramics with greatly improved mechanical properties prepared by low temperature hot-pressing, *Mater. Sci. Eng., A*, 2015, **633**, 194–199.

14 D. Wei, Q. Meng and D. Jia, Microstructure of hot-pressed h-BN/Si_3N_4 ceramic composites with Y_2O_3–Al_2O_3 sintering additive, *Ceram. Int.*, 2007, **33**, 221–226.

15 J. L. Qi, J. H. Lin, J. L. Guo and Y. L. Liu, Plasma treatment on SiO_{2f}/SiO_2 composites for their assisted brazing with Nb, *Vacuum*, 2016, **123**, 136–139.

16 J. H. Lin, D. L. Luo, S. L. Chen and D. S. Mao, Control interfacial microstructure and improve mechanical properties of TC_4-SiO_{2f}/SiO_2 joint by AgCuTi with Cu foam as interlayer, *Ceram. Int.*, 2016, **42**, 16619–16625.

17 J. Place and M. Thomas, *US pat.*, 4786548, 1988.

18 D. C. Jia, L. Z. Zhou, Z. H. Yang, X. M. Duan and Y. Zhou, Effect of Preforming Process and Starting Fused SiO_2 Particle Size on Microstructure and Mechanical Properties of Pressurelessly Sintered BNp/SiO_2 Ceramic Composites, *J. Am. Ceram. Soc.*, 2011, **94**, 3552–3560.

19 G. Wen, G. L. Wu, T. Q. Lei, Y. Zhou and Z. X. Guo, Co-enhanced SiO_2–BN ceramics for high-temperature dielectric applications, *J. Eur. Ceram. Soc.*, 2000, **20**, 1923–1928.

20 X. M. Duan, D. C. Jia, Z. Wang, D. L. Cai, Z. Tian, Z. H. Yang, P. G. He, S. J. Wang and Y. Zhou, Influence of hot-press sintering parameters on microstructures and mechanical properties of h-BN ceramics, *J. Alloys Compd.*, 2016, **684**, 474–480.

21 P. F. Zhang, D. C. Jia, Z. H. Yang, X. M. Duan and Y. Zhou, Influence of ball milling parameters on the structure of the mechanically alloyed SiBCN powder, *Ceram. Int.*, 2012, **38**, 6399–6404.

22 B. Liang, Z. H. Yang, J. C. Rao, D. L. Cai, X. M. Duan, D. C. Jia, Y. Zhou, D. L. Yu, Y. J. Tian and R. Riedel, Highly dense amorphous Si_2BC_3N monoliths with excellent mechanical properties prepared by high pressure sintering, *J. Am. Ceram. Soc.*, 2015, **98**, 3782–3787.

23 J. X. Xue, J. X. Liu and B. H. Xie, Pressure-induced preferential grain growth, texture development and anisotropic properties of hot pressed hexagonal boron nitride ceramics, *Scr. Mater.*, 2011, **65**, 966–969.

24 S. Taruta, R. Fujisawa and K. Kitajima, Preparation and mechanical properties of machinable alumina/mica composites, *J. Eur. Ceram. Soc.*, 2006, **26**, 1687–1693.

25 A. Kalemtas, G. Topates, O. Bahadir, P. Kayaisci and H. Mandal, Thermal properties of pressureless melt infiltrated AlN–Si–Al composites, *Trans. Nonferrous Met. Soc. China*, 2013, **23**, 1304–1313.

26 W. D. Kingery, Factors affecting thermal stress resistance of ceramic materials, *J. Am. Ceram. Soc.*, 1955, **38**, 3–15.

27 L. Chen, Y. J. Wang, H. F. Shen, J. C. Rao and Y. Zhou, Effect of SiC content on mechanical properties and thermal shock resistance of BN–ZrO_2–SiC composites, *Mater. Sci. Eng., A*, 2014, **590**, 346–351.

28 Z. Hou, F. Ye, L. Liu, Q. Liu and H. Zhang, Effects of solid content on the phase assemblages, mechanical and dielectric properties of porous α-SiAlON ceramics fabricated by freeze casting, *Ceram. Int.*, 2013, **39**, 1075–1079.

29 B. W. Sheldon, E. Y. Sun, S. R. Nutt and J. J. Brennan, Oxidation of BN-coated SiC fibers in ceramic matrix composites, *J. Am. Ceram. Soc.*, 1996, **79**, 539–543.

30 V. Lavrenko and A. Alexeev, High-temperature oxidation of boron nitride, *Ceram. Int.*, 1986, **12**, 25–31.

31 M. Westwood, J. Webster, R. Day, F. Hayes and R. Taylor, Oxidation protection for carbon fiber composites, *J. Mater. Sci.*, 1996, **31**, 1389–1397.

32 S. Ray, Derivation of Lichtenecker's logarithmic mixture formula from Maxwell's equations, *IEEE Trans. Microwave Theory Tech.*, 2010, **58**, 545–550.

33 Ceramic properties databases of the American Ceramic Society, http://www.matweb.com/search/SpecificMaterial.aspbassnum.